Title: Decoding individualized motor cortical excitability states from whole-brain electroencephalography

Running title: Decoding cortical excitability

Authors: Sara J Hussain[1]* and Romain Quentin[2]

Affiliations: [1]Movement and Cognitive Rehabilitation Science Program, Department of Kinesiology and Health Education, University of Texas at Austin. Austin, TX, USA.
[2]COPHY Team, Lyon Neuroscience Research Center (CRNL), INSERM, CRNS, Université Claude Bernard Lyon 1, Lyon, France.

***Corresponding Author:**
Sara J Hussain, PhD
540 Bellmont Hall
2109 San Jacinto Blvd
Austin, TX 78712
Email: sara.hussain@austin.utexas.edu
Phone: 847-309-5189

Conflicts of Interest: The authors declare no competing financial interests.

Acknowledgements: Data included in this publication were acquired at the Human Cortical Physiology and Neurorehabilitation Section (directed by Leonardo Cohen) at NINDS.

Funding: This research did not receive any specific grant from funding agencies in the public, commercial, or not-for-profit sectors.

Highlights

- Individual subjects exhibit unique brain activity patterns that predict low and high motor cortex (M1) excitability states.
- Motor-evoked potentials elicited during high excitability states were larger than those elicited during low excitability states.
- Excitability states lasted for seconds at a time, indicating compatibility with brain state-dependent stimulation.

Abstract

OBJECTIVE: Brain state-dependent transcranial magnetic stimulation (TMS) requires real-time identification of cortical excitability states. Here, we aimed to identify individualized, subject-specific motor cortex (M1) excitability states from whole-scalp electroencephalography (EEG) signals.

METHODS: We analyzed a pre-existing dataset that delivered 600 single TMS pulses to the right M1 during EEG and electromyography (EMG) recordings. Subject-specific multivariate pattern classification was used to discriminate between brain states during which TMS elicited small or large motor-evoked potentials (MEPs).

RESULTS: Classifiers trained at the individual subject level successfully discriminated between low and high M1 excitability states. MEPs elicited during classifier-predicted high excitability states were significantly larger than those elicited during classifier-predicted low excitability states. Classifiers trained on subject-specific data obtained immediately before TMS delivery performed better than classifiers trained on data from earlier time points, and subject-specific classifiers generalized weakly but significantly across subjects.

CONCLUSION: Decoding individualized M1 excitability states from whole-brain EEG activity is feasible and robust.

SIGNIFICANCE: Deploying subject-specific classifiers during brain state-dependent TMS may enable effective, fully individualized neuromodulation in the future.

Keywords

machine learning, brain stimulation, transcranial magnetic stimulation, motor cortex

1. Introduction

Over the past few decades, transcranial magnetic stimulation (TMS) has emerged as a potential treatment for a variety of brain disorders, including depression (George et al. 1995; O'Reardon et al. 2007), substance use disorders (Gorelick et al. 2014; Hanlon et al. 2018; Ekhtiari et al. 2019), memory problems (Wang et al. 2014; Nilakantan et al. 2019), and motor impairment caused by neurological damage (Tazoe and Perez 2015; Hummel and Cohen 2006; Webster et al. 2006). Although early work reported that different patterns of repetitive TMS significantly alter primary motor cortex (M1) excitability (Pascual-Leone et al. 1994; Chen et al. 1997; Stefan et al. 2000; Huang et al. 2005), such interventions have since been shown to exhibit weak effect sizes and wide inter- and intra-individual variability (Ziemann and Siebner 2015; Goldsworthy et al. 2021), with in some cases less than half of tested individuals showing the expected plastic response (López-Alonso et al. 2014).

Brain state-dependent TMS may improve homogeneity of TMS effects by delivering TMS during periods of increased cortical excitability and thus increased sensitivity to LTP-like plasticity (Kraus et al. 2016; Kraus et al. 2018; Zrenner et al. 2018; Baur et al. 2020). Recently, TMS has been applied during brain states shown at the group level to correlate with M1 excitability. For example, TMS has been delivered to M1 during sensorimotor rhythm desynchronization (Kraus et al. 2016; Kraus et al. 2018) and during sensorimotor mu trough phases (Zrenner et al. 2018; Baur et al. 2020; Hussain et al. 2021), both of which reflect increased M1 spiking rates (Haegens et al. 2011). Results from this work have been promising: TMS interventions applied during high excitability brain states potentiate corticospinal excitability (Kraus et al. 2016; Kraus et al. 2018; Zrenner et al. 2018; Baur et al. 2020) and enhance motor memory (Hussain et al. 2021) more than identical interventions applied during low excitability brain states.

Nonetheless, current brain state-dependent TMS approaches pose some challenges. Most notably, a reliable high excitability brain state must first be detected across a range of individuals. This can be difficult, as shown by several recent studies reporting inconsistent relationships between the sensorimotor mu rhythm and corticospinal excitability (Sauseng et al. 2009; Berger et al. 2014; Zrenner et al. 2018; Hussain et al. 2019a; Madsen et al. 2019; Bergmann et al. 2019, see Madsen et al. 2019 for summary). Further, maximizing the beneficial effects of brain state-dependent TMS requires this state to correlate with excitability in each individual. Excluding those who do not show such a correlation is also problematic, as it limits the generalizability of results and may artificially inflate effect sizes by screening out potential

“non-responders” ahead of time (Madsen et al. 2019). Other obstacles include difficulty extracting the target brain state in all individuals (Zrenner et al. 2020), a problem that will only be exacerbated in clinical studies involving patients with brain lesions (Hussain et al. 2020) or other forms of volumetric brain loss.

Here, we developed an alternative approach that exploits the rich spatiotemporal dynamics embedded within human EEG signals to predict M1 excitability states in individual subjects. Using multivariate pattern classification, we show that classifiers trained at the individual subject level successfully discriminate between brain states associated with low and high M1 excitability. Our findings demonstrate that identifying individualized cortical excitability states from human EEG recordings is both feasible and robust, representing a key step towards fully individualized, decoding-based brain state-dependent TMS in the future.

2. Materials and Methods

2.1. Human subjects

Data analyzed in this study have been published previously (Hussain et al. 2019a; Hussain et al. 2019b) and are publicly available (https://openneuro.org/datasets/ds002094). The original study (N = 20 healthy subjects, 6 F and 14 M, age 30 ± 1.59 years) involved simultaneous single-pulse transcranial magnetic stimulation (TMS), electroencephalography (EEG), and electromyography (EMG) in 20 healthy subjects. Original study procedures were approved by the National Institutes of Health Combined Neuroscience Section Institutional Review Board and conformed to local regulations for human subjects research. All subjects provided their written informed consent prior to participation. The original study involved a 5 minute eyes-open resting EEG recording followed by application of 600 single TMS pulses during EEG and EMG recordings (see Hussain et al. 2019a for additional methodological details). Only those data acquired during TMS application are presented here.

2.2. Data acquisition

2.2.1. EEG and EMG signal acquisition. EEG signals were recorded using TMS-compatible amplifiers (BrainAmp MR+, BrainVision; sampling rate = 5 kHz, hardware filtering = DC – 1 kHz, resolution 0.5 µV). EEG impedances were maintained below 12 kΩ throughout all recordings. Bipolar EMG signals were recorded using adhesive electrodes arranged in a belly-tendon montage (Signal, Cambridge Electronic Design; sampling rate = 5 kHz, hardware filtering = 5 Hz – 2 kHz).

2.2.2. TMS. TMS was applied as previously reported (Hussain et al. 2019a; Hussain et al. 2019b). Briefly, monophasic, posterior-to-anterior current TMS (MagStim 200^2, MagStim Co. Ltd) was applied over the scalp hotspot for the left first dorsal interosseous muscle (L. FDI) using a figure-of-eight coil. After determining resting motor threshold (RMT) using an automatic threshold-tracking algorithm (Adaptive PEST procedure; Awiszus and Borckhardt 2011), 6 blocks of 100 single TMS pulses were applied to the L. FDI hotspot at 120% RMT (inter-stimulus interval = 5 s with 15% jitter). Breaks were taken during each block when requested by the subject or in response to TMS coil overheating. TMS coil position was monitored for accuracy using frameless neuronavigation throughout the experiment (BrainSight, Rogue Research).

2.3. Data and statistical analysis

2.3.1. EMG processing. EMG signals acquired during single-pulse TMS delivery were used to calculate MEP amplitudes, which served as an objective marker of M1 excitability. EMG data were analyzed using custom-written scripts in MATLAB combined with FieldTrip (Oostenveld et al. 2011). EMG data were segmented from 25 ms to 100 ms after TMS delivery, demeaned, and linearly detrended. Residual EMG offset was removed by subtracting the average EMG amplitude between 1 and 20 ms before TMS delivery from the entire timeseries signal. Trials containing MEPs contaminated by voluntary motor activity were identified as those that contained (1) pre-stimulus EMG root-mean-square values exceeding an individually-defined upper limit (75th percentile + 3 * the inter-quartile range) or (2) MEP signals that poorly correlated with the average MEP signal observed in that subject (Pearson's correlation, right-tailed, $r < 0.4$). In each remaining trial, the peak-to-peak MEP amplitude was calculated as the difference between the maximum and minimum voltage deflection between 20 and 40 ms after each TMS pulse. Low and high M1 excitability states were defined at the individual subject level as those brain states during which single-pulse TMS delivery elicited an MEP with an amplitude in the top or bottom 50% of all observed MEP amplitudes, respectively (i.e., median split).

2.3.2. EEG preprocessing. EEG signals preceding single-pulse TMS delivery were used to calculate spectral power across a range of frequencies. Resulting spectral power values were used as features when building subject-specific classifiers. EEG data were analyzed using custom-written scripts in MATLAB combined with FieldTrip (Oostenveld et al. 2011). EEG signals acquired during single-pulse TMS delivery were segmented from 3.005 to 0.005 s before

TMS delivery. Data from TP9 and TP10 were removed due to poor scalp electrode contact; thus, 28 channels remained for analysis (FP1, FP2, F3, F4, C3, C4, P3, P4, O1, O2, F7, F8, T7, T8, P7, P8, Fz, Cz, Pz, Iz, FC1, FC2, CP1, CP2, FC5, FC6, CP5, and CP6). Data for all remaining channels were re-referenced to the common average reference, demeaned, linearly detrended, notch filtered to remove line noise (zero-phase shift Butterworth filter, order = 4, stop band = 58 to 62 Hz), and downsampled to 500 Hz to reduce computational load. Power spectra were calculated for six 500 ms windows leading up to each TMS pulse (windows included 3.005 – 2.505 s, 2.505 – 2.005 s, 2.005 – 1.505 s, 1.505 – 1.005 s, 1.005 – 0.505 s and 0.505 – 0.005 s before TMS) using Welch's method (4-100 Hz with 0.25 Hz resolution). Power spectral estimates were averaged within each frequency band separately for each of the six windows. This created 168 EEG features per window (i.e., 28 EEG channels for each of 6 different frequency bands). Features included broadband (4-100 Hz), theta (4-7 Hz), alpha (8-12 Hz), beta (13-35 Hz), low gamma (36-60 Hz), and high gamma (61-100 Hz) power.

2.3.3. Single-trial classification at the individual subject level. Multivariate pattern analysis (MVPA) was performed using the MVPA-light toolbox for MATLAB (Treder et al. 2020) combined with custom-written scripts. We first aimed to predict whether an MEP elicited by a single TMS pulse was either small or large (see *EMG processing)* using information contained within power spectral features obtained immediately preceding each pulse (0.505 – 0.005 s before TMS; see *EEG preprocessing*). To achieve this, we used Linear Discriminant Analysis (LDA) with stratified k-fold cross-validation (k = 10). For each subject, the LDA classifier was fit to a training subset of EEG features (9/10ths of all available trials per subject). This allowed the classifier to find the hyperplane that best separated the low and high excitability states. The resulting classifier was then used to predict whether a given trial's MEP belonged to either the low or high excitability state using a separate testing subset of the EEG features (remaining $1/10^{th}$ trials). These steps were performed for each fold, generating a predicted excitability state for each trial's MEP. We calculated the area under the receiver-operator curve (AUC, 1 = perfect classification) by comparing this prediction to each MEP's ground truth class. AUC values and classifier weights were averaged across folds. On average, 552.75 ± 8.45 trials were available for classification per subject. Training and testing sets were always independent, and folds were stratified to ensure approximately equal state representation. Prior to classification, grid search was performed to optimize each subject's lambda value (100 linearly spaced lambda values ranging from 1e-50 to 1). Optimal lambda values were 0.23 ± 0.08 and were used for all classification analyses. Subject-specific confusion matrices indicating the proportion

of accurate and inaccurate classifications were calculated and averaged across subjects to obtain a single group-level confusion matrix.

Classification performance was evaluated statistically at the individual subject and group levels. For individual subjects, statistical significance was determined using permutation tests. State labels (high or low) were randomly shuffled and a new classifier was trained to discriminate between the resulting shuffled states. Performance of this new classifier was evaluated using AUC values. This process was repeated 10,000 times to obtain a subject-specific null distribution of AUC values. If a given subject's true AUC value exceeded the 95th percentile of the null distribution (analogous to a right-tailed statistical test with alpha = 0.05), above-chance classification was considered to have occurred. At the group level, statistical significance was evaluated by comparing the group-level distribution of true AUC values to the standard chance level for a two-class classification problem (chance = 0.5). All statistical testing (other than permutation tests) was performed using right-tailed Wilcoxon signed rank tests. Kolmogorov-Smirnoff tests were used to confirm non-normality and alpha was equal to 0.05 for all analyses.

To confirm that subject-specific classifiers correctly identified low and high M1 excitability states, we also compared amplitudes of MEPs evoked during classifier-predicted low excitability states and classifier-predicted high excitability states. At the individual level, MEP amplitudes were compared between predicted low and high states using a left-tailed Mann Whitney U-test. The U-test was used instead of the Wilcoxon signed rank test to account for potentially unequal trial numbers per class. At the group level, MEP amplitudes were averaged within each state per subject and then compared using a left-tailed Wilcoxon signed rank test. Left-tailed statistical tests were used to test the *a priori* hypothesis that MEPs elicited during low excitability states would be smaller than those elicited during high excitability states. Kolmogorov-Smirnoff tests were used to confirm non-normality and alpha was equal to 0.05 for all analyses.

Directly interpreting classifier weights describing the hyperplane that optimally separates low and high excitability states can lead to inaccurate localization of neural activity underlying successful classification (Haufe et al. 2014). To identify the spatial distribution of features most strongly contributing to successful classification in each subject, we transformed classifier weights into spatial activation patterns by multiplying them with the noise covariance matrix (Haufe et al. 2014). Spatial activation patterns associated with subject-specific classification

using all 168 features (corresponding to results presented in Figure 1) are depicted in Supplementary Figures 1-6.

2.3.4. Contribution of band-limited features to classification performance. The extent to which different power spectral features contributed to classification performance was evaluated in two ways. Subject-specific classification was performed using the same method described above (see *Single-trial classification at the individual subject level*), except that classifiers were fit for single feature sets describing either broadband power, theta power, alpha power, beta power, low gamma power, or high gamma power. For this analysis, only the time window immediately preceding TMS (0.505 – 0.005 s before TMS) was used. This resulted in six classifiers per subject. AUC values obtained for classifiers trained on each feature set were compared to chance using right-tailed FDR-corrected (Benjamini and Hochberg 1995) Wilcoxon signed rank tests. AUC values for each classifier were compared using pairwise FDR-corrected two-tailed Wilcoxon signed rank tests. Kolmogorov-Smirnoff tests were used to confirm non-normality and alpha was equal to 0.05 for all analyses.

Second, the extent to which adding additional features affected classification performance was evaluated. For each subject, a first classifier was fit using broadband power features only. Then, the remaining feature sets (theta, alpha, beta, low gamma, and high gamma power) were added in a step-wise manner, so that six classifiers, each with 28 more features than the previous one (corresponding to the 28 channels), were fit per subject. AUC values obtained from each classifier were compared to chance using FDR-corrected right-tailed Wilcoxon signed rank tests. Given that classifiers trained using broadband power features only performed better than classifiers trained using only theta, alpha, beta, low gamma, or high gamma features (see Figure 2a), AUC values for classifiers trained using broadband power features only were compared to those trained using broadband power features plus each additional feature set using pairwise FDR-corrected two-tailed Wilcoxon signed rank tests. Kolmogorov-Smirnoff tests were used to confirm non-normality and alpha was equal to 0.05 for all analyses.

2.3.5. Single-trial generalization of classifiers across subjects. We then tested whether classifiers trained at the individual subject level using features calculated from EEG data immediately preceding TMS delivery (0.505 – 0.005 s before TMS) generalized across all other subjects. Classifiers trained at the single-subject level (using all 168 features; see *EEG preprocessing* and *Single-trial classification at the individual subject level*) were used to

discriminate between low and high excitability states in all other subjects. Generalization performance was assessed using AUC values. Because classifiers were trained on one subject and tested on all others, training and testing sets were always independent and no stratification was used.

Generalization performance was evaluated at the individual subject and group levels. For individual subjects, AUC values reflecting the extent to which each subject's individual classifier generalized to all other test subjects was compared to chance. At the group level, AUC values were averaged across all 19 test subjects per training subject. This created a distribution of aggregate generalization AUC values, which were then also compared to chance. Finally, aggregate generalization AUC values were compared to AUC values obtained during single-trial classification at the individual level. All statistical testing was performed using right-tailed Wilcoxon signed rank tests. Kolmogorov-Smirnoff tests were used to confirm non-normality and alpha was equal to 0.05 for all analyses.

2.3.6. Evaluation of classification performance across time. To determine if classifiers performed differently when using EEG features obtained from earlier time windows preceding TMS, we applied the same subject-specific classification approach described above (see *Single-trial classification at the individual subject level*). Here, subject-specific classifiers were instead trained and tested using all 168 power spectral features obtained from EEG signals obtained within five different 500 ms windows preceding TMS (3.005 –2.505 s, 2.505 – 2.005 s, 2.005 – 1.505 s, 1.505 – 1.005 s, 1.005 – 0.505 s before TMS). Classification performance at each time point was evaluated statistically by comparing group-level AUC values to chance using right-tailed FDR-corrected Wilcoxon signed rank tests. We then used pairwise FDR-corrected Wilcoxon signed rank tests to determine if each time point's AUC values exceeded the AUC values obtained from classifiers trained using EEG features obtained immediately before TMS delivery (0.505 – 0.005 s before TMS). Because results of this analysis revealed above-chance classification performance at all tested time points (see *Results*), we further asked whether the information used to achieve successful classification in earlier time windows (3.005 –2.505 s, 2.505 – 2.005 s, 2.005 – 1.505 s, 1.505 – 1.005 s, 1.005 – 0.505 s before TMS) was the same information used to achieve successful classification immediately preceding TMS (0.505 – 0.005 s before TMS). This was done by testing the extent to which subject-specific classifiers trained on all 168 power spectral features obtained from EEG data immediately preceding TMS generalized to earlier time points. AUC values describing the extent to which each subject's

trained classifier generalized backwards in time were thus calculated (King and Dehaene 2014). Group-level temporal generalization performance was evaluated by comparing AUC values at each time point to AUC values obtained during subject-specific classification using features calculated from EEG data within 0.505 – 0.005 s before TMS using right-tailed FDR-corrected Wilcoxon signed rank tests. Kolmogorov-Smirnoff tests were used to confirm non-normality and alpha was equal to 0.05 for all analyses.

3. Results

We first determined if classifiers trained at the individual subject level successfully discriminated between low and high M1 excitability states using features obtained from EEG data immediately preceding TMS delivery (168 features calculated from EEG data within 0.505 to 0.005 s before TMS). At the individual level, 17 of 20 subjects showed above-chance classification performance ($p < 0.04$ for all) while performance for the remaining three subjects did not exceed chance ($p > 0.06$ for all). Group-level classification performance was also significantly higher than chance ($p < 0.001$; Figure 1a). The group-level confusion matrix revealed that accurate classification occurred more often than inaccurate classification (Figure 1b, yellow versus blue cells), with overall AUC values of 0.58 ± 0.01 (range = 0.48 – 0.63). MEP amplitudes elicited during classifier-predicted high excitability states were significantly larger than those elicited during classifier-predicted low excitability states in 16 of 20 subjects ($p < 0.04$ for all), while in the remaining four subjects this was not the case ($p > 0.05$ for all). At the group level, MEP amplitudes were 14.13 ± 2.70% larger when evoked during classifier-predicted high versus low excitability states ($p < 0.001$, Figure 1c).

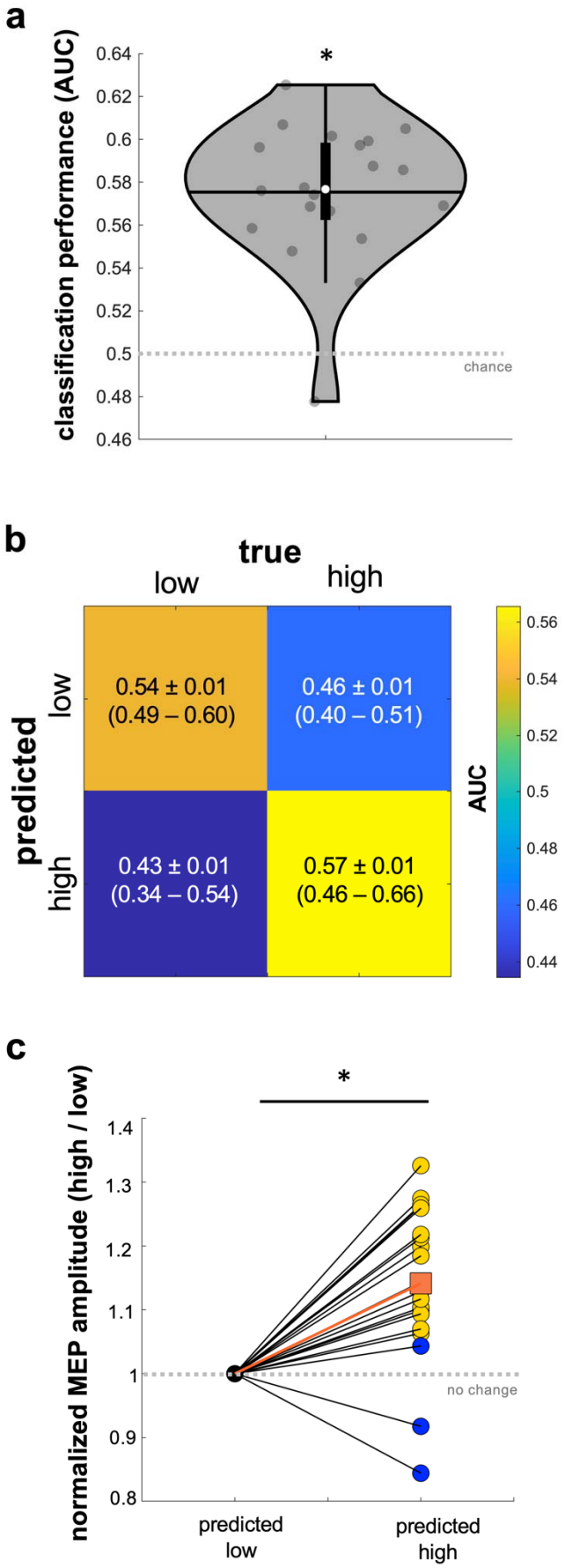
a
classification performance (AUC)
0.64
0.62
0.6
0.58
0.56
0.54
0.52
0.5
0.48
0.46
*
chance
b
true
low
high
predicted
low
high
0.54 ± 0.01
(0.49 – 0.60)
0.46 ± 0.01
(0.40 – 0.51)
0.43 ± 0.01
(0.34 – 0.54)
0.57 ± 0.01
(0.46 – 0.66)
AUC
0.56
0.54
0.52
0.5
0.48
0.46
0.44
c
normalized MEP amplitude (high / low)
1.4
1.3
1.2
1.1
1
0.9
0.8
*
no change
predicted
low
predicted
high

Figure 1. Subject-specific classification of low and high M1 excitability states. a) AUC values reflecting classification performance. Classifiers were trained at the individual subject level using 168 features obtained from EEG data immediately preceding TMS (i.e., between 0.505 and 0.005 s before TMS). These classifiers performed significantly above chance in 17 of 20 subjects and at the group level. Grey dots = individual subject AUC values, thick whisker = interquartile range, thin whisker = full range, white dot = group median, black horizontal line = group mean. The grey dotted line indicates the standard chance level for a two-class classification problem. b) Group-level confusion matrix describing the proportion of accurate and inaccurate classifications of M1 excitability states. Horizontal and vertical dimensions indicate predicted and ground truth states, respectively. Note that the proportions of true low (upper left) and true high (lower right) classifications exceed the proportions of false low (upper right) and false high (lower left) classifications. Error estimates are SEM, with the observed range across subjects indicated in parentheses. c) MEP amplitudes elicited during classifier-predicted low (black dot) and high (yellow/blue dots) M1 excitability states. Before plotting, MEPs were normalized by dividing those obtained during high excitability states by those obtained during low excitability states for each subject. MEPs were significantly larger during classifier-predicted high excitability states in 16 of 20 subjects (yellow dots) and at the group level. Blue dots indicate subjects for whom MEPs were not significantly larger during classifier-predicted high versus classifier-predicted low states. The orange square indicates the group mean MEP amplitude during classifier-predicted high excitability states, normalized to the group mean MEP amplitude during classifier-predicted low excitability states. The dashed grey line reflects no change in MEP amplitudes. * group-level statistical significance.

We next evaluated the contribution of specific power spectral features to classification performance, again using features calculated from EEG data obtained immediately preceding TMS delivery (0.505 – 0.005 s before TMS). In addition to classifiers trained using all 168 features (see Figure 1a), those trained with only a single set of 28 band-limited power features successfully discriminated between low and high M1 excitability states ($p < 0.01$ for all, Figure 2a). Classification performance further depended on the specific features used, with classifiers trained using only broadband power features significantly outperforming those trained using only theta, alpha, beta, and high gamma power features ($p < 0.02$ for all), but not those trained using only low gamma power features ($p = 0.06$). In addition, classification performance remained above chance as additional features were added to an initial classifier trained using only broadband power features ($p < 0.001$ for all, Figure 2b), but including these additional features did not significantly improve performance ($p > 0.14$ for all pairwise comparisons).

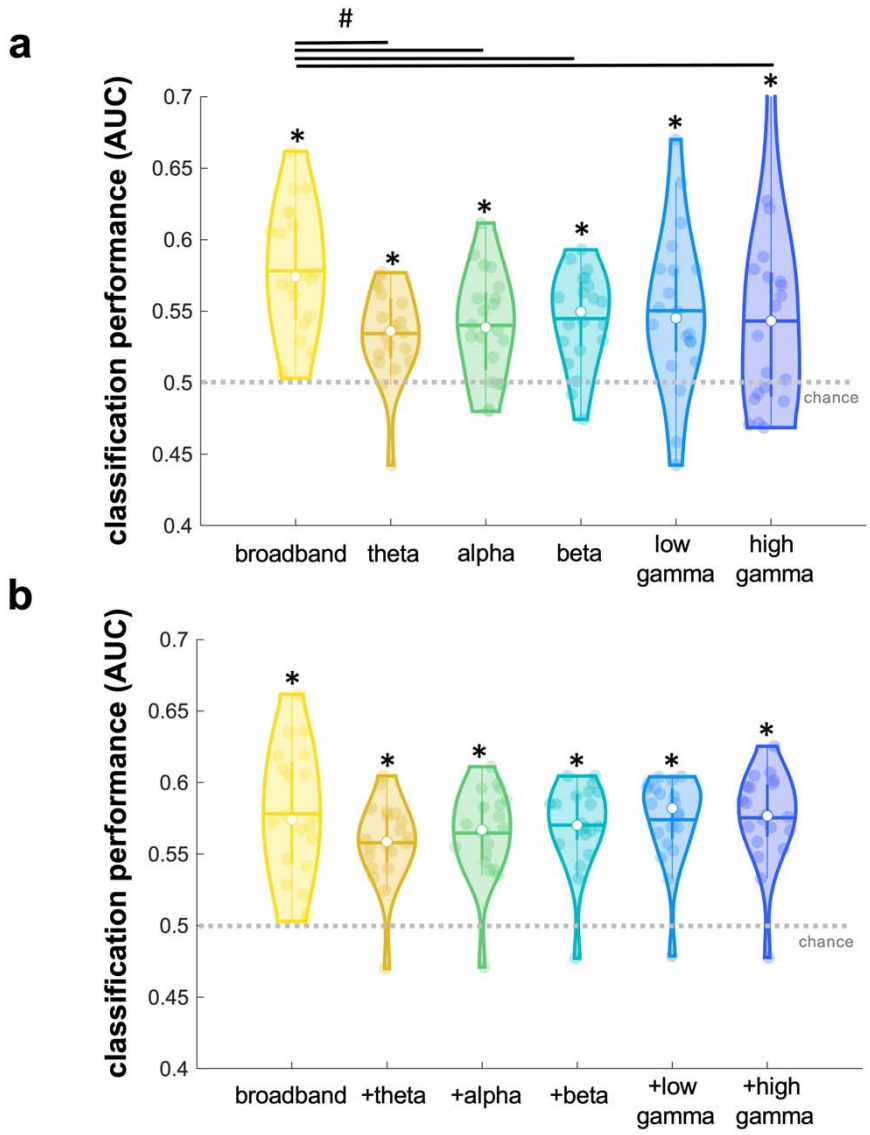

Figure 2. Contribution of power spectral features to classification performance. a) AUC values reflecting performance of classifiers trained using single sets of power spectral features obtained from EEG signals immediately preceding TMS delivery (0.505 – 0.005 s before TMS). All six classifiers performed significantly above chance at the group level. Classifiers trained using broadband power features significantly outperformed classifiers trained using only theta, alpha, beta, and high gamma power features but not those trained using only low gamma power features. b) AUC values reflecting performance of classifiers with step-wise addition of different power spectral feature sets calculated from EEG data obtained immediately before TMS delivery (0.505 – 0.005 s before TMS). All six classifiers again performed significantly above chance at the group level, but performance did not improve as additional power spectral features were added to an original classifier trained using broadband power features only. For both panels, colored dots = individual subject AUC values, thick whiskers = interquartile ranges, thin whiskers = full ranges, white dots = group medians, colored horizontal lines = group means. The grey dotted lines indicate the standard chance level for a two-class classification problem. * statistical significance of AUC values when compared to chance. # statistical significance of pairwise comparisons.

Next, we examined whether subject-specific classifiers trained using all 168 features calculated from EEG signals immediately preceding TMS (0.505 to 0.005 s before TMS) generalized across subjects. Classifiers trained in four of 20 subjects showed above chance performance when tested on the remaining 19 subjects (see Figure 3a for subject-level generalization matrix, $p < 0.04$ for all) while the remaining 16 subjects did not ($p > 0.10$ for all). This corresponded to group-level generalization performance AUC values of 0.51 ± 0.003 (range = 0.47 – 0.52, Figure 3b), which significantly exceeded chance ($p = 0.02$). Yet, generalization performance was still significantly worse than subject-specific classification performance ($p < 0.001$, see also Figure 1a).

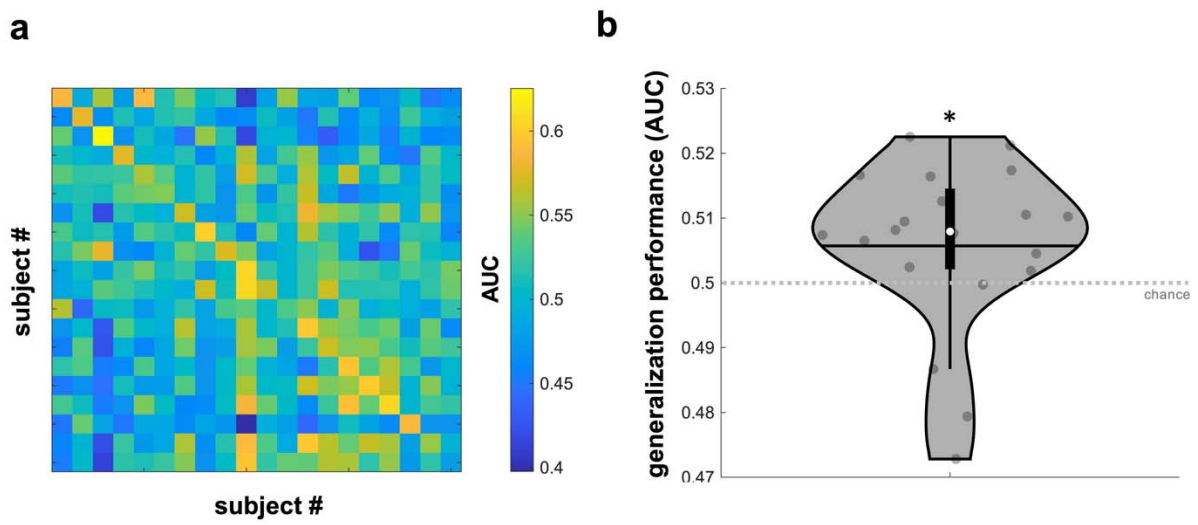

Figure 3. Cross-subject generalization of subject-specific classifiers. a) Matrix of AUC values reflecting cross-subject generalization performance of classifiers trained using all 168 features obtained from EEG signals immediately preceding TMS (0.505 – 0.005 s before TMS). The diagonal reflects AUC values obtained from individual subject classification (i.e., diagonal values match those presented in Figure 1a). Warmer and coolor colors indicate higher and lower AUC values, respectively. b) AUC values indicating generalization performance averaged across all testing subjects per training subject. AUC values exceeded chance in 4 of 20 subjects and also at the group level. Grey dots = individual subject AUC values, thick whisker = interquartile range, thin whisker = full range, white dot = group median, black horizontal line = group mean. The grey dotted line indicates the standard chance level for a two-class classification problem. * statistical significance of AUC values when compared to chance.

Finally, we evaluated the temporal evolution of classification performance over 3 seconds leading up to TMS delivery. Classifiers trained and tested on all features extracted from EEG data within each pre-TMS window (3.005 –2.505 s, 2.505 – 2.005 s, 2.005 – 1.505 s, 1.505 – 1.005 s, 1.005 – 0.505 s before TMS) showed above-chance performance (Figure 4a, $p < 0.002$ for all). However, classifier performance was higher immediately before TMS delivery than at any other time point ($p < 0.03$ for all). Further, AUC values of classifiers trained using features obtained immediately before TMS delivery (0.505 – 0.005 s before TMS) and tested on each of the preceding time windows also exceeded chance ($p < 0.001$ for all; Figure 4b). Classification AUC values obtained using features calculated from EEG data immediately preceding TMS delivery (i.e., 0.505 – 0.005 s before TMS) were significantly higher than generalization AUC values obtained from 3.005 – 2.505 s, 2.505 – 2.005 s, 2.005 – 1.505 s, and 1.505 – 1.005 s before TMS ($p < 0.03$ for all). Generalization AUC values at all other time points did not differ significantly from classification AUC values obtained from 0.505 – 0.005 s before TMS ($p > 0.09$ for all).

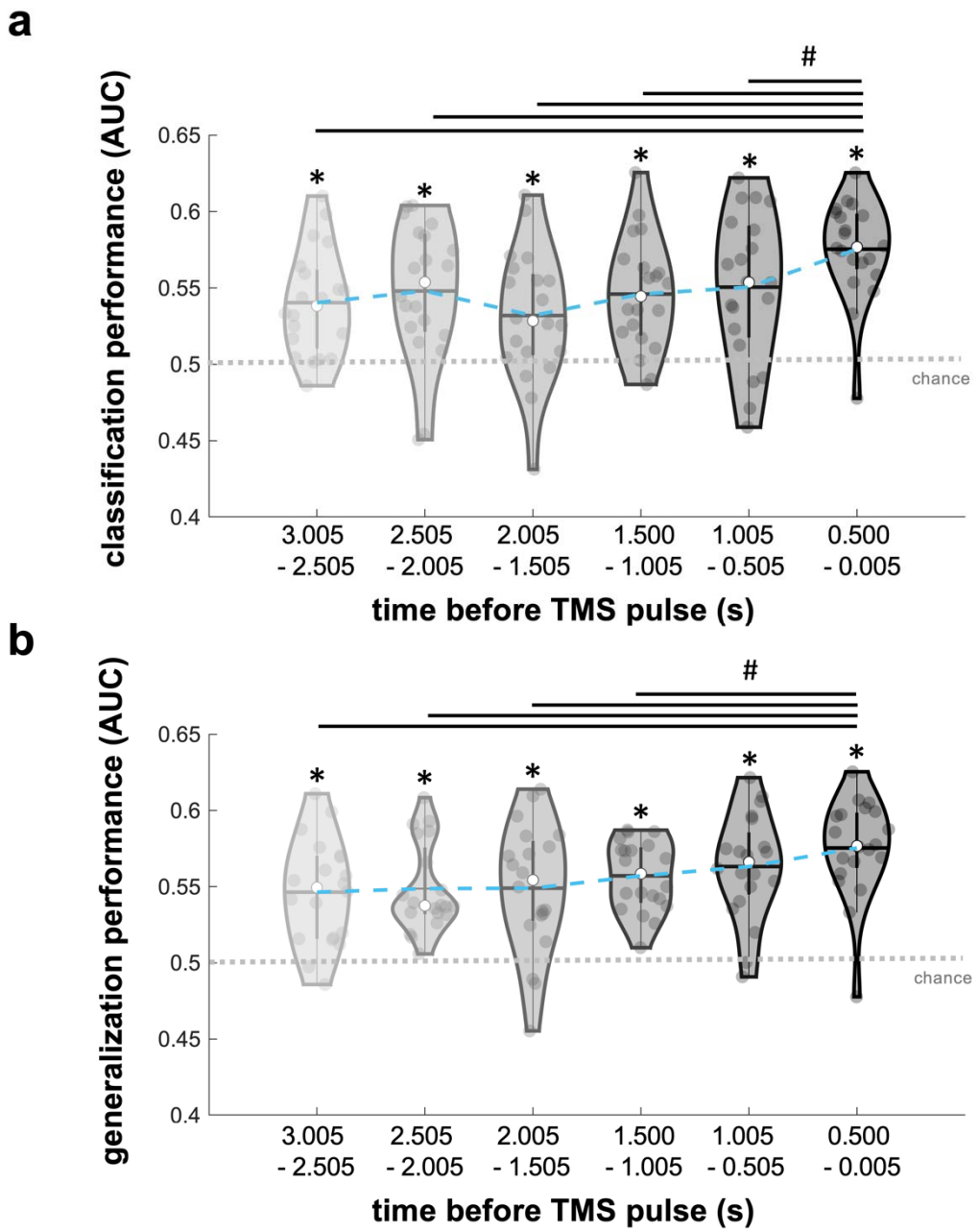

Figure 4. Evaluation of classification performance over time. a) AUC values reflecting performance of classifiers trained and tested using power spectral features obtained from EEG data in different time windows preceding TMS delivery. Classification AUC values for the time point closest to TMS delivery (0.500 – 0.005 s before TMS) were significantly higher than classification AUC values obtained for all other tested time points. b) AUC values reflecting the extent to which subject-specific classifiers trained using power spectral features obtained from EEG data immediately before TMS delivery (0.500 – 0.005 s, far right) generalized to earlier time points. Classification AUC values for the time point closest to TMS delivery (0.500 – 0.005 s before TMS) were significantly higher than generalization AUC values for the four time points

furthest from TMS delivery (3.005 – 2.505, 2.505 – 2.005, 2.005 – 1.505, and 1.505 – 1.005 s before TMS). Note that for both panels, the data depicted on the right-most violin plot reflects subject-specific classification AUC values (also depicted in Figure 1a). Time windows used to calculate power spectral features are depicted on the x axes. Blue dashed lines indicate group-level AUC values approaching TMS delivery. Grey dots = individual subject AUC values, thick whisker = interquartile range, thin whisker = full range, white dot = group median, grey/black horizontal lines = group mean. The grey dotted line indicates the standard chance level for a two-class classification problem. * statistical significance of AUC values when compared to chance. # statistical significance of pairwise comparisons.

4. Discussion

In this study, we used multivariate pattern analysis to identify individualized M1 excitability states using whole-scalp EEG recordings. We found that classifiers trained at the individual subject level successfully discriminated between low and high M1 excitability states. These states were associated with an ~14% difference in MEP amplitudes. Further, classifiers trained at the individual subject level generalized weakly but significantly across subjects. Overall, classifiers performed best when subject-specific EEG features obtained within ~ 500 ms of TMS delivery were used to predict M1 excitability.

Historically, TMS has been delivered to the brain irrespective of ongoing brain activity. Early studies showed that TMS protocols using different stimulation rates and burst patterns induce either LTP- or LTD-like plasticity within human M1 (Pascual-Leone et al. 1994; Chen et al. 1997; Stefan et al. 2000; Huang et al. 2005). However, more recent reports suggest that the plastic effects of TMS interventions may depend more strongly on the excitability state at the time of stimulation than the specific pulse rate or pattern (Zrenner et al. 2018; Baur et al. 2020), consistent with findings in animal models (Pavlides et al. 1988; Huerta and Lisman 1993; Huerta and Lisman 1995; Zanos et al. 2018). For example, whether hippocampal stimulation induces LTP or LTD critically depends on the theta phase (which is closely tied to hippocampal excitability, Buzsáki 2002) at the exact moment of stimulation (Pavlides et al. 1998; Huerta and Lisman 1993; Huerta and Lisman 1995). Accumulating evidence thus suggests that TMS protocols are most likely to induce LTP- and LTD-like plasticity when delivered during high and low excitability states, respectively, motivating development of effective and generalizable methods capable of predicting their occurrence (Kraus et al. 2016; Kraus et al. 2018; Zrenner et al. 2018; Madsen et al. 2019; Shirinpour et al. 2020). Along these lines, current state-of-the-art methods use oscillatory properties shown at the group level to correlate with excitability levels (Zrenner et al. 2018; Madsen et al. 2019; Baur et al. 2020; Hussain et al. 2020; Hussain et al. 2021), but approaches capable of predicting cortical excitability in a fully individualized manner

have not yet been developed. Here, we introduce a novel decoding-based framework that identifies subject-specific M1 excitability states from whole-scalp EEG signals.

A major advantage of the decoding-based approach described here is its fully individualized nature. Because of this, it does not require *a priori* knowledge of the group-level relationship between cortical excitability and EEG activity. Instead, it discovers subject-specific brain states associated with low versus high M1 excitability using machine learning. The fact that we successfully identified M1 excitability states in 85% of subjects using power spectral features obtained from only 28-channel EEG recordings illustrates the strength of this method. Increasing the spatial resolution of recordings via high-density electrode arrays and/or incorporating more complex features (i.e., coherence or other functional connectivity estimators) could further improve performance. Due to its individualized nature, the decoding-based approach presented here in principle also does not require any specific cortical morphometry. This characteristic makes it particularly well-suited for brain state-dependent TMS in patients with cortical stroke (Hussain et al. 2020) or other forms of brain damage.

The decoding-based framework presented here is also compatible with real-time application. As data are acquired and spectrally decomposed in real-time, a spatial filter generated from weights of a pre-trained classifier can be used to identify the occurrence of brain states associated with low and high M1 excitability. Our results showed that EEG data obtained up to 3 seconds before TMS delivery successfully discriminated between low and high M1 excitability states, indicating that these states last for seconds at a time. Thus, TMS could in the future simply be triggered upon real-time state detection. Such an approach contrasts starkly with computationally-intensive phase-dependent TMS algorithms that use autoregressive forward prediction to estimate the instantaneous oscillatory phase at some future time point (Zrenner et al. 2018; Madsen et al. 2019; Baur et al. 2020; Shirinpour et al. 2020; Hussain et al. 2021) and are much easier to implement (see Bergmann et al. 2012). Further, the amount of MEP modulation seen here (~14%) closely matches that observed when using phase-dependent M1 TMS (Zrenner et al. 2018; Hussain et al. 2019a; Bergmann et al. 2019; Baur et al. 2020), suggesting similar efficacy despite a reduced computational load.

Classifiers trained at the individual subject level generalized significantly but weakly across subjects when examined at the group level. Despite group-level statistical significance, such generalization was only present in 20% of subjects. Further, classification at the individual

subject level outperformed cross-subject generalization and only exceeded chance by a very small amount (mean AUC = ~ 0.51; chance level = 0.50). These results indicate the importance of subject-specific information when predicting M1 excitability. Indeed, subject-specific features can explain up to half of the variance in time-varying brain activity (Gratton et al. 2018) and such activity can reliably identify individual subjects (Finn et al. 2015). Given these previous reports, it is perhaps not surprising that individualized brain activity patterns also predict M1 excitability. Still, whether the brain states identified here are stable across multiple recording sessions has yet to be established. Determining the magnitude of cross-session generalization will be important for future decoding-based brain state-dependent TMS applications.

The current findings also demonstrate the contribution of broadband power and whole-brain activity to M1 physiology. First, we found that spectral features describing power within any of the canonical frequency bands (i.e., theta, alpha, etc.) were sufficient for successful classification, but classifiers that used broadband power features typically performed best. Adding additional features to classifiers that used broadband power only did not improve their performance, suggesting that broadband power is particularly useful when predicting M1 excitability. Along these lines, previous invasive recording studies showed that broadband power is a more robust marker of population-level neuronal spiking than band-limited power (Manning et al. 2009) and that its dynamics track finger movements within human M1 (Miller et al. 2012). Broadband power signals also correlate with blood oxygen level-dependent responses obtained via fMRI (Pan et al. 2011; Winawer et al. 2013; Wen and Liu 2016), emphasizing their close relationship to other, more conventional cortical activation measures. Our findings and these previous reports suggest that broadband power reflects a robust yet still underutilized marker of human M1 excitability that is easily accessible with EEG. Second, our results convincingly show that whole-brain activity predicts the presence of low and high M1 excitability states (see Supplementary Figures 1-6 for individual subject activation patterns). Although most previous work has focused on the relationship of local sensorimotor rhythms to M1 excitability (Kraus et al. 2016; Kraus et al. 2018; Zrenner et al. 2018; Hussain et al. 2019a; Madsen et al. 2019; Bergmann et al. 2019), M1 excitability is also dynamically shaped by cognitive processes (including attention and alertness, Rösler et al. 1999; Noreika et al. 2020) that rely on neural activity within areas upstream of M1 (Bestmann and Krakauer 2015). However, because here TMS was delivered while subjects were not engaged in any cognitive task and brain activity was recorded using 28-channel EEG that precludes reliable source localization (Michel and Brunet 2019), we are unable to make any claims regarding the cognitive

and/or anatomical origins of the excitability states described here. Future work using higher-density EEG combined with source localization and/or attentional manipulations could uncover the mechanistic underpinnings of whole brain-M1 interactions.

In conclusion, we report that individual subjects exhibit unique brain activity patterns associated with M1 excitability and that these patterns can be successfully decoded from whole-scalp EEG signals. Classifier-identified brain states reflected a ~14% change in MEP amplitudes and lasted for seconds at a time, making them ideal targets for brain state-dependent TMS. Overall, the framework presented here constitutes a key step towards flexible, fully individualized decoding-based brain state-dependent TMS in the future.

References

Baur D, Galevska D, Hussain S, Cohen LG, Ziemann U, Zrenner C. (2020). Induction of LTD-like corticospinal plasticity by low-frequency rTMS depends on pre-stimulus phase of sensorimotor μ-rhythm. *Brain Stimul* 13(6):1580-1587.

Benjamini Y, Hochberg Y. (1995). Controlling the false discovery rate: a practical and powerful approach to multiple testing. *J Royal Stat Soc: Methodological* 57(1):289-300.

Berger B, Minarik T, Liuzzi G, Hummel FC, Sauseng P. (2014). EEG oscillatory phase-dependent markers of corticospinal excitability in the resting brain. *BioMed Res Intl* 2014:936096.

Bergmann TO, Lieb A, Zrenner C, Ziemann U. (2019). Pulsed facilitation of corticospinal excitability by the sensorimotor μ-alpha rhythm. *J Neurosci* 39(50):10034-10043.

Buzsáki G. (2002). Theta oscillations in the hippocampus. *Neuron* 33(3):325-340.
Chen RM, Classen J, Gerloff C, Celnik P, Wassermann E, Hallett M, Cohen LG. (1997). Depression of M1 excitability by low-frequency transcranial magnetic stimulation. *Neurology* 48(5):1398-1403.

Ekhtiari H, Tavakoli H, Addolorato G, Baeken C, Bonci A, Campanella S, Castelo-Branco L, Challet-Bouju G, Clark VP, Claus E, Dannon PN, Felice AD, den Uyl T, Diana M, di Giannantonio M, Fedota JR, Fitzgerald P, Gallimberti L, Hanlon CA. (2019). Transcranial electrical and magnetic stimulation (tES and TMS) for addiction medicine: a consensus paper on the present state of the science and the road ahead. *Neurosci Biobehav Rev* 104:118-140.

Finn ES, Shen X, Scheinost D, Rosenberg MD, Huang J, Chun MM, Papademetris X, Constable TR. (2015). Functional connectome fingerprinting: identifying individuals using patterns of brain connectivity. *Nat Neurosci* 18(11):1664-1671.

George MS, Wassermann EM, Williams WA, Callahan A, Ketter TA, Basser P, Hallett M, Post RM. (1995). Daily repetitive transcranial magnetic stimulation (rTMS) improves mood in depression. *NeuroReport* 6(14):1853-1856.

Goldsworthy MR, Hordacre B, Rothwell JC, Ridding MC. (2021). Effects of rTMS on the brain: is there value in variability?. *Cortex* 139:43-59.

Gorelick DA, Zangen A, George MS. (2014). Transcranial magnetic stimulation (TMS) in the treatment of substance addiction. *Ann New York Acad Sci* 1327(1):79.

Gratton C, Laumann TO, Nielsen AN, Greene DJ, Gordon EM, Gilmore AW, Nelson SM, Coalson RS, Snyder AZ, Schalggar BL, Dosenbach NU. (2018). Functional brain networks are dominated by stable group and individual factors, not cognitive or daily variation. *Neuron* 98(2):439-452.

Haegens S, Nácher V, Luna R, Romo R, Jensen O. (2011). α-Oscillations in the monkey sensorimotor network influence discrimination performance by rhythmical inhibition of neuronal spiking. *Proc Natl Acad Sci* 108(48):19377-19382.

Hanlon CA, Dowdle LT, Henderson JS. (2018). Modulating neural circuits with transcranial magnetic stimulation: implications for addiction treatment development. *Pharmacol Rev* 70(3):661-683.

Haufe S, Meinecke F, Görgen K, Dähne S, Haynes JD, Blankertz, B., & Bießmann, F. (2014). On the interpretation of weight vectors of linear models in multivariate neuroimaging. *NeuroImage* 87:96-110.

Huang YZ, Edwards MJ, Rounis E, Bhatia KP, Rothwell JC (2005). Theta burst stimulation of the human M1. *Neuron* 45(2):201-206.

Hummel FC, Cohen LG. (2006). Non-invasive brain stimulation: a new strategy to improve neurorehabilitation after stroke? *The Lancet Neurology* 5(8):708-712.

Huerta PT, Lisman JE. (1993). Heightened synaptic plasticity of hippocampal CA1 neurons during a cholingergically induced rhythmic state. *Nature* 364(6439):723-725.

Huerta PT, Lisman JE. (1995). Bidirectionally synaptic plasticity induced by a single burst during cholingergic theta oscillation in CA1 in vitro. *Neuron* 15(5):1053-1063.

Hussain SJ, Claudino L, Bönstrup M, Norato G, Cruciani G, Thompson R, Zrenner C, Ziemann U, Buch ER, Cohen LG. (2019a). Sensorimotor oscillatory phase–power interaction gates resting human corticospinal output. *Cereb Cortex* 29(9):3766-3777.

Hussain SJ, Hayward W, Fourcand F, Zrenner C, Ziemann U, Buch ER, Cohen LG. (2020). Phase-dependent transcranial magnetic stimulation of the lesioned hemisphere is accurate after stroke. *Brain Stimul* 13(5):1354-1357.

Hussain, SJ, Cohen LG, Bönstrup M. (2019b). Beta rhythm events predict corticospinal motor output. *Sci Rep* 9(1):1-10.

Hussain SJ, Vollmer MK, Stimely J, Norato G, Zrenner CZ, Ziemann U, Buch ER, Cohen LG. (2021). Phase-dependent offline enhancement of human motor memory. *Brain Stimul* 14(4):873-883.

Kraus D, Naros G, Bauer R, Leão MT, Ziemann U, Gharabaghi A. (2016). Brain–robot interface driven plasticity: distributed modulation of corticospinal excitability. *NeuroImage* 125:522-532.

Kraus D, Naros G, Guggenberger R, Leão MT, Ziemann U, Gharabaghi A. (2018). Recruitment of additional corticospinal pathways in the human brain with state-dependent paired associative stimulation. *J Neurosci* 38(6):1396-1470.

King JR, Dehaene S. (2014). Characterizing the dynamics of mental representations: the temporal generalization method: *Trends Cog Sci* 18(4):203-210.

López-Alonso V, Cheeran B, Río-Rodríguez D, Fernández-del-Olmo M. (2014). Inter-individual variability in response to non-invasive brain stimulation paradigms. *Brain Stimul* 7(3):372-380

Madsen KH, Karabanov AN, Krohne LG, Safeldt MG, Tomasevic L, Siebner HR. (2019). No trace of phase: Corticomotor excitability is not tuned by phase of pericentral mu-rhythm. *Brain Stimul* 12(5):1261-1270.

Manning, JR, Jacobs J, Fried I, Kahana M. (2009). Broadband shifts in local field potential power spectra are correlated with single-neuron spiking in humans. *J Neurosci* 29(43):13613-13620.

Michel CM, Brunet D. (2019). EEG source imaging: a practical review of the analysis steps. *Front Neurol* 10:325.

Miller KJ, Hermes D, Honey CJ, Hebb AO, Ramsey NF, Knight RT, Ojemann JG, Fetz EE. (2012). Human M1 activity is selectively phase-entrained on underlying rhythms. *PLoS Comput Biol* 8(9):e1002655.

Nilakantan AS, Mesulam MM, Weintraub S, Karp EL, VanHaerents S, Voss JL. (2019). Network-targeted stimulation engages neurobehavioral hallmarks of age-related memory decline. *Neurology* 92(20):e2349-e2354.

Noreika V, Kamke MR, Canales-Johnson A, Chennu S, Bekinschtein TA, Mattingley JB. (2020). Alertness fluctuations when performing a task modulate cortical evoked responses to transcranial magnetic stimulation. *NeuroImage* 223:117305.

O'Reardon JP, Solvason HB, Janicak PG, Sampson S, Isenberg KE, Nahas Z, McDonald WM, Avery D, Fitzgerald PB, Loo C, Demitrack MA, George MS, Sackeim H. A. (2007). Efficacy and safety of transcranial magnetic stimulation in the acute treatment of major depression: a multisite randomized controlled trial. *Biol Psychiatry* 62(11): 1208-1216.

Oostenveld R, Fries P, Maris E, Schoffelen JM. (2011). FieldTrip: open source software for advanced analysis of MEG, EEG, and invasive electrophysiological data. *Compu Intell Neurosci* 2011:156869.

Rösler KM, Etter C, Truffert A, Hess CW, Magistris MR. (1999). Rapid cortical motor output map changes assessed by the triple stimulation technique. *Neuroreport* 10(3):579-583/

Pan WJ, Thompson G, Magnuson M, Majeed W, Jaeger D, Keilholz S. (2011). Broadband local field potentials correlate with spontaneous fluctuations in functional magnetic resonance

imaging signals in the rat somatosensory cortex under isoflurane anesthesia. *Brain Connectivity* 1(2):119-131.

Pascual-Leone A, Valls-Solé J, Wassermann EM, Hallett M. (1994). Responses to rapid-rate transcranial magnetic stimulation of the human M1. *Brain* 117(4):847-858.

Pavlides C, Greenstein YJ, Grudman M, Winson J. (1988). Long-term potentiation in the dentate gyrus is induced preferentially on the positive phase of θ-rhythm. *Brain Res* 439(1-2):383-387.

Sauseng P, Klimesch W, Gerloff C, Hummel FC. (2009). Spontaneous locally restricted EEG alpha activity determines cortical excitability in M1. *Neuropsychologia* 47(1):284-288.

Shirinpour S, Alekseichuk I, Mantell K, Opitz A. (2020). Experimental evaluation of methods for real-time EEG phase-specific transcranial magnetic stimulation. *J Neural Eng* 17(4):046002.

Stefan K, Kunesch E, Cohen LG, Benecke R, Classen J. (2000). Induction of plasticity in the human M1 by paired associative stimulation. *Brain* 123(3):572-584.

Tazoe T, Perez MA. (2015). Effects of repetitive transcranial magnetic stimulation on recovery of function after spinal cord injury. *Arch Phys Med Rehabil* 96(4):S145-S155.

Treder MS. (2020). MVPA-Light: a classification and regression toolbox for multi-dimensional data. *Front Neurosci* https://doi.org/10.3389/fnins.2020.00289

Wang JX, Rogers LM, Gross EZ, Ryals AJ, Dokucu ME, Brandstatt KL, Hermiller MS, Voss JL. (2014). Targeted enhancement of cortical-hippocampal brain networks and associative memory. *Science* 345(6200):1054-1057.

Webster BR, Celnik PA, Cohen LG. (2006). Noninvasive brain stimulation in stroke rehabilitation. *NeuroRx* 3(4):474-481.

Wen H, Liu Z. (2016). Broadband electrophysiological dynamics contribute to global resting-state fMRI signal. *J Neurosci* 36(22):6030-6040.

Winawer J, Kay KN, Foster BI, Rauschecker AM, Parvizi J, Wandell BA. (2013). Asynchronous broadband signals are the principal source of the BOLD response in human visual cortex. *Curr Biol* 23(13):1145-1153.

Zanos S, Rembado I, Chen D, Fetz EE. (2018). Phase-locked stimulation during cortical beta oscillations produces bidirectional synaptic plasticity in awake monkeys. *Curr Biol* 28(16):2515-2526.

Ziemann U, Siebner HR. (2015). Inter-subject and inter-session variability of plasticity induction by non-invasive brain stimulation: boon or bane?. *Brain Stimul* 8(3):662-663.

Zrenner C, Desideri D, Belardinelli P, Ziemann U. (2018). Real-time EEG-defined excitability states determine efficacy of TMS-induced plasticity in human M1. *Brain Stimul* 11(2):374-389.

Zrenner C, Galveska D, Nieminen JO, Baur D, Stefanou MI, Ziemann U. (2020). The shaky ground truth of real-time phase estimation. *NeuroImage* 214:116761.